GT2021-58883

Comparison of CFD predictions of supercritical carbon dioxide axial flow turbines using a number of turbulence models

AbdElRahman AbdElDayem[1], Martin T. White[1], Abdulnaser I. Sayma[1]
[1]Thermo-Fluids Research Centre, School of Mathematics, Computer science and Engineering,
City, University of London. EC1V 0HB, United Kingdom.

ABSTRACT

A detailed loss assessment of an axial turbine stage operating with a supercritical carbon dioxide (sCO$_2$) based mixture, namely titanium tetrachloride (CO$_2$-TiCl$_4$ 85-15%), is presented. To assess aerodynamic losses, computational fluid dynamics (CFD) simulations are conducted using a geometry generated using mean-line design equations which is part of the work delivered to the SCARABEUS project [1]. The CFD simulations are 3D steady state and employ a number of turbulence models to investigate various aerodynamic loss mechanisms. Two categories of turbulence models are used: Eddy Viscosity and Reynold's Stress models (RSM). The Eddy Viscosity models are the k-ε, k-ε RNG, k-ω, k-ω SST and k- ω Generalized while the RSM models are BSL, LRR, w-RSM and k-ε EARSM. The comparison between different turbulence models showed minor deviations in mass-flow rate, power output and blade loading while significant deviations appear in the loss coefficients and the degree of reaction. It is noted that the k-ε model gives the highest loss coefficients and the lowest isentropic efficiencies while most of the RSM models indicate higher efficiencies and lower loss coefficients. At off-design conditions a sensitivity study revealed that the k-ε RNG model records the sharpest drop in the isentropic efficiency of 8.24% at low mass flowrate reaching 30% off-design. The efficiency sensitivity is found to be less for the other tested models getting 3.1% drop in efficiency for the LRR RSM model.

Keywords: Axial Turbines, Loss estimation, Turbulence modelling, Supercritical CO$_2$.

NOMENCLATURE

BSL	Base line
c	Absolute velocity (m/s)
DOR	Degree of Reaction
$EARSM$	Explicit Algebraic Reynold's Stress Model
h	Enthalpy (J/kg)
LRR	Launder Reece Rodi
$\dot{m}$	Mass flow rate (kg/s)
P	Pressure (Pa)
RNG	Renormalized Group
RSM	Reynold's Stress Model
s	Entropy (J/(kg.K))
t	Time (s)
T	Temperature (K)
u	Mean blade linear velocity (m/s)
w	Relative velocity (m/s)
Z	Blade loading factor

Greek Symbols

γ	Pressure loss coefficient
η_{tt}	Total-to-total efficiency
η_{ts}	Total-to-static efficiency
ξ_N	Nozzle loss coefficient
ξ_R	Rotor loss coefficient

Subscripts

01	Inlet state, total conditions
02	Interface state, total conditions
2	Actual interface state.
2s	Isentropic interface state.
03	Outlet total conditions
3	Actual outlet state
3s	Isentropic outlet state at interface entropy
3ss	Isentropic outlet state at inlet entropy

1 INTRODUCTION

Turbines are critical components within power generation cycles and the overall cycle thermal efficiency is highly dependent on their performance. In large scale power cycles, axial turbines are preferred because they can reach higher efficiencies at higher specific speeds compared to radial inflow designs. Recent studies have recommended the application of

supercritical carbon dioxide (sCO_2) as the working fluid within power generation cycles, as an alternative to traditional working fluids such as steam and air [2]. Potential applications include nuclear power, concentrated-solar power (CSP) and waste-heat recovery, within which the characteristics of carbon dioxide have the advantage of potentially achieving higher cycle efficiencies. Moreover, sCO_2 is denser than other fluids, which facilitates very compact turbomachinery, and hence plants with small physical footprints, to be realised.

Transcritical CO_2 power cycles have also been introduced in the literature where the thermal efficiency can be enhanced compared to supercritical cycles by conducting the compression process in the liquid phase with a lower compression work. In transcritical power cycles, the cooling process takes place at a pressure lower than the critical pressure of the working fluid and continues until the working fluid is completely condensed. The critical temperature of pure CO_2 is approximately 31 ºC which is relatively low compared to the atmospheric temperature in hot countries where CSP applications are more viable which can reach up to 40 ºC. This means achieving condensation with dry cooling is infeasible. For this reason, CO_2 mixtures have been introduced as alternatives to pure CO_2. The addition of a dopant could raise the critical temperature of the CO_2 based mixture to a value exceeding the temperature of available cooling streams, allowing condensation at ambient temperature in a typical solar field.

Different CO_2 based mixtures have been tested and evaluated in the literature. However, titanium tetrachloride ($TiCl_4$) has been selected for this study due to its potential to achieve high thermal efficiencies. Manzolini *et al.* [3] presented a techno-economic assessment of two different CO_2 based mixtures for CSP power plants, namely $TiCl_4$ and di-nitric tetroxide (N_2O_4). The analysis showed that the thermal efficiency can reach 43% and 50% with maximum cycle temperatures of 550 and 700 ºC respectively using the proposed mixtures, achieving a 2% increase in thermal efficiency compared to pure CO_2. $TiCl_4$ has been also considered by Bonalumi *et al.* [4], [5] in which a critical temperature for the CO_2-$TiCl_4$ mixture of up to 45 ºC was achieved, which is sufficiently high for condensation in hot countries.

Once the working fluid and cycle operating conditions have been determined, the turbine can be designed using mean-line design methods [6], and the performance of the turbine can be evaluated. Different types of mechanical and aerodynamic losses are expected to be present in large scale axial turbines although this paper considers only aerodynamic losses. The aerodynamic losses include tip clearance, secondary flow, partial admission, trailing edge, shock, incidence, external leakage and exit losses.

The tip clearance loss is the loss due to mass leaking from the gap between the rotating blades and the fixed casing causing loss in power. It is critical especially in high reaction stages where the pressure difference across the rotor blades is high [7]. Secondary flows can be defined as undesired flow streams passing through the turbine stage generating turbulence and introducing flow features such as passage, counter and horse

shoe vortices [8]. The trailing edge contributes to entropy generation due to the sharp transition in the flow area at the blade trailing edge. Denton and Xu [9] stated that the trailing edge losses are minor and can be neglected in subsonic flow although they increase significantly as the flow becomes supersonic. The exit losses are defined as the kinetic energy of the exiting flow stream which cannot be recovered.

An overall estimation of different losses has been presented by Trindade *et al.* [10] who reviewed existing loss models for high pressure axial turbines operating under off-design conditions. The investigated models were Dunham & Came [11], Kacker & Okapuu [12], Craig & Cox [13], and Moustapha [14]. The results of these models were compared to experimental data which showed an over estimation of stator profile loss coefficient in all the models. Ennil *et al.* [15], [16] evaluated the applicability of loss models working with both large- and small-scale axial turbines. To assess the loss models, a CFD loss evaluation for a small-scale axial air turbine was conducted using the k-ω SST turbulence model. The results were compared to different loss models from the literature, namely: Ainely & Mathieson model [17], Dunham & Came, and Kacker & Okapuu models. Results showed that the Kacker & Okapuu model predicted the closest values to the CFD simulation results.

CFD simulation is widely applied to turbomachinery to evaluate performance and characterise sources of loss across a range of operating conditions. For a defined geometry, working fluid and set of boundary conditions, results of flow, pressure, and temperature fields are determined by solving the mass, momentum, and energy equations with the addition of turbulence models to simulate flow near the wall. Turbulence models are a set of equations that are used to simplify the turbulence flow structure, which is highly irregular and unsteady in nature. To fully capture this behaviour very fine mesh sizes and 3D unsteady models are necessary to capture fine eddies and vortices resulting from turbulent flow. These simulations are called Direct Numerical simulations (DNS) which require a very high computational power to be solved and are impractical for assessing the performance of a turbine stage. Fortunately, alternatives such as Large Eddy Simulations (LES) or the Reynolds Average Navier Stokes (RANS) models can be employed which represent the eddies and fine vortices as averaged velocity and pressure fields and are known to provide accurate predictions of the flow behaviour.

LES solves the flow equations in an unsteady 3D form where large scale turbulent motion can be captured, whilst RANS models reduce the turbulent flow completely to averaged flow quantities. LES generally gives better accuracy compared to RANS models and requires less computational time compared to DNS, however, its application is limited to large swirl and external flow applications. Thus, RANS remains the most common approach applied to turbomachinery.

RANS turbulence models are defined using a set of equations to determine the unknown turbulent correlations needed for the Reynolds Average Navier Stokes (RANS) equations. These models vary in complexity level and can be

classified as Eddy Viscosity Models and Reynolds Stress Models. Eddy Viscosity Models are based on "Boussinesq hypothesis" which relates the turbulent stresses to the mean velocity gradients similar to the relation between the viscous stresses and the complete velocity gradients [18]. Eddy viscosity models can be classified into zero, one, two, three or four equation models according to the number of equations used to determine the eddy viscosity term for the Reynold's stress equations. The two equation eddy viscosity models are the most common, especially k-ε and k-ω models. Reynolds Stress Models (RSM) closes the Reynolds-Averaged Navier-Stokes equations by solving additional transport equations for the six independent Reynolds stresses plus one equation for the turbulence dissipation. Compared to eddy viscosity models, RSM models are more complex and require more computational power to be solved, however they are the most appropriate for complex flows. RSM models release the assumption made with eddy viscosity models by avoiding isotropic eddy viscosity making these models more suitable for high swirl motion, rotation, and high strain rates [19].

CFD contributions are presented throughout the literature using various turbulence models for turbomachinery using different working fluids like steam, air and sCO₂. Jang *et al.* [7] used the k-ω SST turbulence model to simulate a multi-stage ultra-supercritical steam turbine. Comparing the predicted mass-flow rates and pressure ratios to the provided data by the turbine manufacturer showed that this method is effective in simulating axial turbines. Modified low-Reynolds k-ε and k-ω SST turbulence models were examined by Noori Rahim Abadi *et al.* [20] who conducted a CFD based optimisation of a steam turbine blade. The results showed that the k-ω SST turbulence model is more accurate compared to the standard k-ε model in predicting the wet steam flow field. Francesco *et al.* [21] verified the performance of the realizable k-ε model against available data from the literature for a single row stationary blades running condensing steam. The k-ε RNG model results have been also verified in the literature for a steam turbine [22].

The performance of a small scale gas turbines is studied and presented by Morgese *et al.* [23] who generated a preliminary mean-line model by considering appropriate loss coefficients. The k-ω SST turbulence model is then applied in a 3D CFD simulation to get the actual loss coefficients which are iteratively fed to the mean line design. Within this study, k-ω SST model was found to provide high accuracy in determining loss coefficients of a small-scale axial gas turbine by comparing the CFD results to the experimental data. Touil and Ghenaiet [24] verified the k-ω turbulence model in a two-stage high pressure air turbine.

Supercritical CO₂ turbomachinery are introduced in the literature for both axial and radial turbines however, most of the available studies are for radial-inflow turbines. The performance of a small-scale axial turbine is introduced by Han *et al.* [25] using a CFD model for two turbines rated at 3.28 kW and 6.287 kW, respectively. The proposed CFD model uses k-ω SST as the turbulence model and the results are verified against mean-line thermodynamic design model. The results

have shown a reasonable loading curves, Mach number contours and streamline spectrums. A relatively large-scale axial turbine running sCO₂ is shown by Shi *et al.* [26] who built a thermodynamic model for the initial design of a three-stage 10 MW axial turbine. The results of the thermodynamic model are verified against CFD model using k-ω SST as the turbulence model. For radial inflow turbines, it is found that most of the CFD studies have been conducted using the standard k-ε turbulence model [27, 28] and a few papers have evaluated the k-ω SST model [29]. Zhou *et al.* [27] proposed a CFD model for a sCO₂ radial turbine to investigate both design and off-design conditions with the results showing that the generated power and the efficiency of the turbine was 1.16 MW and 85.36%, respectively. Compared to mean-line design, the largest deviation in the simulation results under the normal design conditions is 3.73%.

Many other CFD contributions are made using various turbulence models where the commonly used turbulence models are the k-ω SST [23, 30-33], the realizable k-ε model [21, 28], k-ε RNG [22], and k-ω model [24]. It can be noted there have been limited studies evaluating Reynold's stress models (RSM), such as the baseline model (BSL RSM), the omega based (ω-RSM), the Launder Reece Rodi model (LRR RSM) or the modified explicit algebraic k-ε model EARSM.

It can be concluded from the literature that comparisons between the performance predictions made using different turbulence models are very limited. Moreover, most of the previous CFD studies have evaluated turbines operating with steam and air, while the performance assessment of axial turbines operating with sCO₂ based mixtures has not been previously addressed. Most of the proposed CFD studies in the literature are limited to covering the most common types of turbulence models like k-ε, k-ω and k-ω SST models neglecting many other available turbulence models without a clear justification of why other models are not considered. In terms of comparing different turbulence models, the maximum number of turbulence models compared within a study is no more than three, and thus the relative performance of different turbulence models in turbomachinery has not been investigated previously in a single study. Given the lack of experimental data relating to sCO₂ turbomachinery, evaluating the sensitivity of the performance predictions made using different turbulence models is considered a necessary step to ensure that robust performance predictions can be made.

In this study, a preliminary turbine design is simulated using several CFD models which are verified against mean-line predictions obtained using Soderberg's correlation. Nine turbulence models are used to simulate the flow characteristics of the sCO₂-TiCl₄ mixture, and these are compared to highlight the differences in performance predictions. The CFD simulations are compared based on performance parameters including loss coefficients, efficiencies and loading coefficient, while the loss distribution along the flow path is investigated. Finally, the behaviour of the turbulence models at off-design conditions is investigated.

2 CFD IMPLEMENTATION

To initiate a CFD simulation, key parameters must firstly be defined. In turbomachines, these parameters are the geometry for the stator/rotor blades, a source for thermo-physical properties of the working fluid, mathematical model for the governing equations and physical phenomena, boundary conditions and solver settings defining the type of the simulation and numerical tolerance.

The applied boundary conditions summarised in Table 1 are extracted from the initial mean-line turbine design provided by City, University of London, in their contribution to the SCARABEUS project [1]. A preliminary cycle modelling and optimisation code running sCO_2-Titanium Tetrachloride (sCO_2-$TiCl_4$) mixture has been developed to identify the optimum dopant mass fraction according to a predefined set of boundary conditions. These conditions are set by the SCARABEUS project according to the project aims and objectives to utilise solar power generated from CSP plants for a transcritical power cycle. Similar cycle modelling techniques have been introduced historically to decide the optimum operating point for the different cycle components which can be subsequently used for the specific components design [34, 35]. The turbine stage considered in this study is the first of a four-stage 50% reaction axial turbine designed to generate approximately 120 MW from the whole turbine using supercritical CO_2 mixture operating in a transcritical power generation cycle. Since the main interest of this study is to evaluate the stage losses and to compare different turbulence models, only the first stage is considered instead of modelling the whole turbine where the objectives of the study can be achieved with minimum computational effort. The geometrical parameters generated from the mean-line design are summarised in Table 2. These parameters are used to generate the 3D blade profile.

TABLE 1 OPERATING CONDITIONS

Parameter	Value
Working Fluid	CO_2-$TiCl_4$
Blend mass fraction	15%
Inlet total pressure	250 bar
Inlet total temperature	700 °C
Inlet turbulence intensity	5% (medium)
Outlet static pressure	198 bar
Hub, shroud, and blade walls	Adiabatic, smooth
Rotational Speed	3000 RPM

A commercial package (SIMULIS) was used to model the fluid properties using the Peng Robinson equation of state with binary interaction coefficients of 0.0745 and 0 as reported in [3]. An in-house code has been developed to generate look-up tables for use by the CFD solver with the pressure ranging from 50 bar to 300 bar and the temperature ranging from 300 K to 1200 K with 200 steps for each. The CFD model is a steady state 3D model of a single stage axial turbine using single flow passages for the stator and rotor. Periodic boundary conditions are applied to both rotor and stator blades. Total pressure, total temperature and turbulence intensity are defined at the inlet boundary of the stationary domain while static pressure is defined for the outlet boundary of the rotor domain. The interface between the fixed and rotating domains is modelled using a mixing plane approach where the average flow data are transferred between upstream and downstream of the interface. No tip clearance is defined within this study.

TABLE 2 GEOMETRY CALCULATED BY MEAN-LINE DESIGN

Blade Angles (deg)	
Stator inlet flow angle	0
Stator outlet flow angle	61.64
Rotor inlet relative flow angle	-5.57
Rotor outlet relative flow angle	62.79
Rotor outlet absolute flow angle	0
Lengths (mm)	
Stator blade axial length	20.66
Rotor blade axial length	17.59
Stator blade chord length	23.86
Rotor blade chord length	20.31
Rotor Stator axial gap	15.00
Radii (mm)	
Rotor hub radius	516.64
Stator inlet tip radius	540.46
Stator outlet tip radius	543.00
Rotor inlet tip radius	543.12
rotor outlet tip radius	545.28
Number of Blades	
Number of stator blades	227
Number of rotor blades	268

ANSYS Turbo Grid software is used to generate a high-quality mesh tailored for turbomachines which applies controlled mesh refinement in the near wall region. The applied mesh sizes are adjusted to suit each turbulence model while automatic wall treatment option is activated to switch between the standard wall function for $30 < y+ < 300$ and the low Reynolds number model for $y^+ < 5$ so that the flow behaviour near the walls is accurately resolved. The y^+ values are monitored at different mesh sizes and kept below 100 in most of the cases to ensure solution accuracy near the walls.

3 LOSS ESTIMATION

The main aim of this paper is to evaluate the performance of a large sale axial turbines operating with CO_2-$TiCl_4$ mixture as the working fluid. Different types of aerodynamic losses are considered by the CFD model such as secondary flow, vortex, trailing edge, partial admission, incidence, shockwave, and windage losses. However, some of these losses have no significant effect on the results due to the proposed case

definition, such as partial admission and incidence losses which are only considered at off-design operating conditions. The windage loss has a minor effect in an axial unshrouded turbine stage and the effect of tip clearance is not considered in this study as the radial gap between the rotor and the shroud surface is omitted to simplify the simulation.

The key aerodynamic losses are therefore due to secondary flows, vortices, and trailing edge losses. The concept of entropy generation is applied to assess the impact of each of these losses. The relation between the axial location and the entropy generation is proposed to give a direct definition to each type of these losses making use of the axial location of each blade row to categorise the entropy distribution for each type of loss accordingly. Within the location of rotor and stator blades, secondary flows are dominating, while the end of each blade passage shows the loss induced by the trailing edge. The region between the rotor and stator, along with the rotor outlet domains, are more affected by turbulence eddies where vortex losses along with secondary flows are dominating. An enthalpy–entropy chart is useful for the purpose of relating the expansion, defined by Δh, to the amount of loss defined by Δs, where a larger gradient (i.e., $\Delta h/\Delta s$) shows a good expansion process with a minimum amount of loss.

To evaluate and compare the various turbulence models, the loss coefficients defined by Equations 1 to 4 are defined, while Equations 5 to 6 provide the definition of the total-to-total efficiency and the total-to-static efficiency.

Nozzle loss coefficient

$$\xi_N = \frac{(h_2 - h_{2s})}{\frac{1}{2}c_2{}^2} \tag{1}$$

Nozzle local loss coefficient

$$\xi = \frac{h - h_s}{h_{01} - h_{2s}} \tag{2}$$

Blade loss coefficient

$$\xi_B = \frac{(h_3 - h_{3s})}{\frac{1}{2}w_3{}^2} \tag{3}$$

Stagnation Pressure loss coefficient

$$\gamma = \frac{(P_{01} - P_{03})}{(P_{03} - P_3)} \tag{4}$$

Total to total efficiency

$$\eta_{tt} = \frac{(h_{01} - h_{03})}{(h_{01} - h_{03ss})} \tag{5}$$

Total to static efficiency

$$\eta_{ts} = \frac{(h_{01} - h_{03})}{(h_{01} - h_{3ss})} \tag{6}$$

In the previous equations, h_2 is the static enthalpy at the nozzle outlet, h_{2s} is the isentropic static enthalpy at the nozzle outlet defined as a function of the nozzle inlet entropy and interface pressure, c_2 is the absolute velocity at the nozzle outlet, h is the local enthalpy at the defined circumferential location, h_s is the local isentropic enthalpy value at the same circumferential location and inlet entropy, h_3 is the static enthalpy at the rotor outlet, h_{3s} is the isentropic static enthalpy at the rotor outlet defined as a function of the rotor inlet entropy and outlet pressure, w_3 is the relative rotor velocity at the outlet, P_{01} is the total pressure at the nozzle inlet, P_{03} is the total pressure at the rotor outlet, P_3 is the static pressure at the rotor outlet, h_{01} is the total enthalpy at the nozzle inlet, h_{03} is the total enthalpy at the rotor outlet, h_{03ss} is the isentropic total enthalpy at the rotor outlet evaluated at the nozzle inlet entropy and the rotor outlet total pressure and h_{3ss} is the isentropic enthalpy at the rotor outlet evaluated at the rotor inlet entropy and the rotor outlet pressure. All velocity and pressure values are area averaged, while thermodynamic properties such as enthalpy and entropy are mass averaged.

The blade loading factor (Z) defined by Equation 7 is used to compare the pressure difference across the rotor blades in different turbulence models:

$$Z = \frac{h_{01} - h_{03}}{u^2} \tag{7}$$

where h_{01} and h_{03} are the total enthalpies at the nozzle inlet and stator outlet respectively and u is the blade linear speed.

The nomenclature for the proposed turbine stage is presented by Figure 1 on a $h\text{-}s$ diagram and velocity diagram.
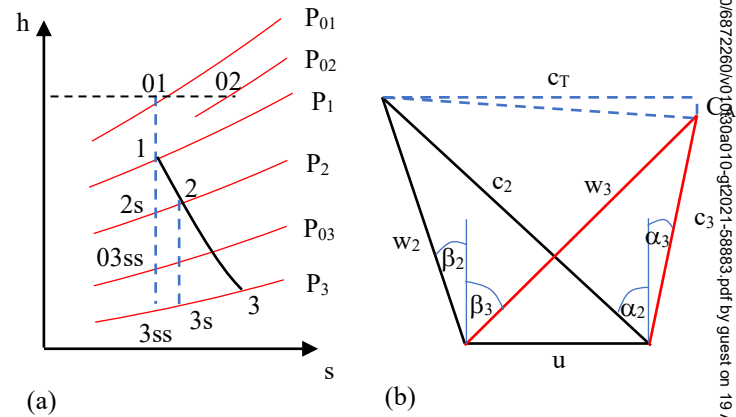

FIGURE 1 NOMENCLATURE FOR (A) h-s DIAGRAM, (B) VELOCITY DIAGRAM

The following section reviews the results for the various loss coefficients obtained for each turbulence model. These results help in showing how the different turbulence models affect the performance of the turbine.

4 RESULTS AND DISCUSSIONS

4.1 CFD verification

The CFD model is setup using the same boundary conditions and geometry generated by the mean-line design. To verify the CFD results, the results are compared to a mean-line loss prediction model based on Soderberg's correlation. The comparison is summarised in Table 3. For the purpose of comparison, the k-ω model, which is commonly used turbulence model in turbomachinery applications [21, 22, 28], is selected to show the differences between the mean-line and CFD results. The results show a good agreement between the two models in mass-flow rate, power, velocities, and efficiencies, while it can be noted that the degree of reaction (DOR) is smaller, and the loss coefficients are larger, for the CFD simulation compared to the mean-line model.

The DOR is calculated as 46.5% and 53.1% for the CFD and mean-line model, respectively. Following further investigation, it was found that the smaller DOR predicted from the CFD simulation implies that the enthalpy drop across the stator blades is larger in the CFD simulation resulting in a higher absolute velocity at the rotor inlet. The differences between the mean-line model and the CFD simulation are expected because the mean-line model only considers a limited set of parameters related to the blade shape ignoring the flow blockage resulting from the physical blades. Some geometrical parameters used to define the 3D blade shape are not considered in the mean-line model, for example the axial gap between stator and rotor, inlet and outlet profiles cone angle, inlet and outlet fillets radii, control points used to define the aerofoil profile of the blades and the radial profile twist along the blade span. These parameters control the flow passage area along the path from inlet to outlet where the expansion process and the degree of reaction are controlled. For the proposed model, the values of blade profile parameters are manually iterated using CFD results to generate a smooth expansion through the turbine stage achieving the required area ratio with minor swirl motion within the flow field. No variation in profile twist is defined along the blade hight because the blade hight in this case is relatively small compared to the blade mean diameter.

The large difference between the estimated loss coefficients by Soderberg and the CFD simulation is due to the fact that Soderberg's correlation only considers the effect of a few parameters, including the Reynold's number and blade aspect ratios, while the actual flow structure and secondary flow streams are not considered. The details of the flow structure and the turbulence along the flow path thus result in differences in the obtained stator and rotor loss coefficients.

A comparison between the velocity triangles obtained for the mean-line and CFD results are reported in Figure 2, which agrees with the data included in Table 3 while the different states represented on h-s diagram are compared in Figure 3.

TABLE 3 COMPARISON BETWEEN THE MEAN-LINE MODEL AND THE k-ω CFD MODEL

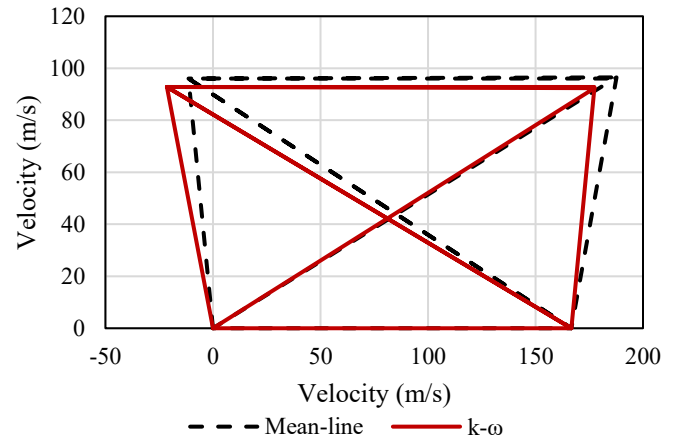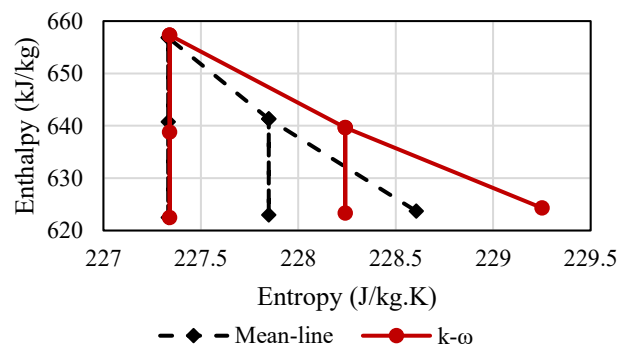|	Mean-line	CFD k-ω	Difference
$\dot{m}$	1111.50	1056.84	-5.2%
$Power$	36.9	35.2	-4.7%
η_{tt}	0.965	0.948	-1.8%
η_{ts}	0.845	0.842	-0.3%
DOR	0.531	0.465	-14.1%
c_1	99.21	94.09	-5.4%
c_2	202.27	209.69	3.5%
c_3	98.76	92.94	-6.3%
w_2	96.75	95.24	-1.6%
w_3	211.04	199.98	-5.5%
ξ_S	0.024	0.039	38.3%
ξ_R	0.032	0.047	32.8%
Z	1.194	1.199	0.4%

FIGURE 2 VELOCITY TRIANGLES

FIGURE 3 COMPARING h-s DIAGRAM FOR THE CFD k-ω MODEL AGAINST THE MEAN-LINE MODEL.

4.2   Mesh refinement

The accuracy of CFD simulations highly depends on the grid structure. The key aim here is to achieve a mesh independent solution for each turbulence model to ensure the differences between each turbulence model are only due to the inherent differences in the governing equations. To ensure a high-quality mesh, different perspectives have been considered including defining the mesh size near the walls to achieve a target Y^+ value as recommended for each turbulence model, varying the global mesh size and growth rate, and finally testing different grids to ensure a mesh independent solution.

To estimate the first element thickness near the blade, hub and shroud walls of the turbine stage, Equation 8 [24] is used as a preliminary tool for setting the mesh size near the walls to ensure that Y^+ values are kept between 30 and 300 the standard wall function within ANSYS is applied. An automatic wall treatment option has been selected for all turbulence models to account for the variation of Y^+ values where the conversion between the standard wall function and low Reynolds's wall functions at very low Y^+ values is allowed. A representative distribution for Y^+, obtained using k-ω turbulence model, is reported in Figure 4 to show how the values vary over the walls.

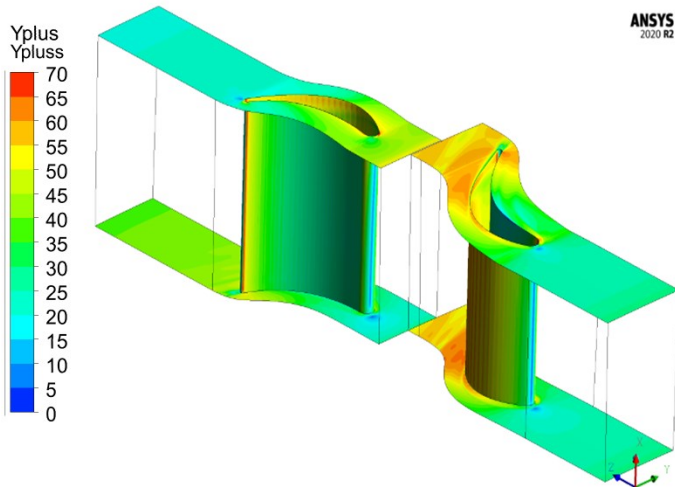$$\Delta y = LY^+\sqrt{80}Re_x^{1/14}Re_L^{-1} \qquad (8)$$

FIGURE 4 Y^+ CONTOURS ON HUB, SHROUD AND BLADE SURFACE OBTAINED BY SOLVING k-ω TURBULENCE MODEL.

The grid generation parameters have also been modified to obtain a high-quality mesh element using small growth rate and suitable grid mapping for each part of the solution domain. Different mesh sizes have been tested to eliminate the effect of changing the mesh size on the solution as indicated by Figure 5, which shows a sample of the mesh independence studies carried out for the nine proposed turbulence models. Figure 5 (a) shows the mesh independence study for the k-ω SST model which achieved a mesh independent solution using the lowest number of grid points, while Figure 5 (b) shows the mesh

independence study for the k-ε EARSM model which showed the largest number of grid points needed for a mesh independent solution.

For the k-ω SST model, it is found that a total number of grid points of 1.29 million is sufficient to reach a mesh independent solution with a total variation in efficiency and power developed of 0.29% and 0.058% respectively relative to the results obtained for the finest mesh. For the k-ε EARSM model, a total number of grid points of 4.23 million is selected as the mesh independent solution where the deviation in efficiency and power developed is found to be 0.1% and 0.06% respectively.
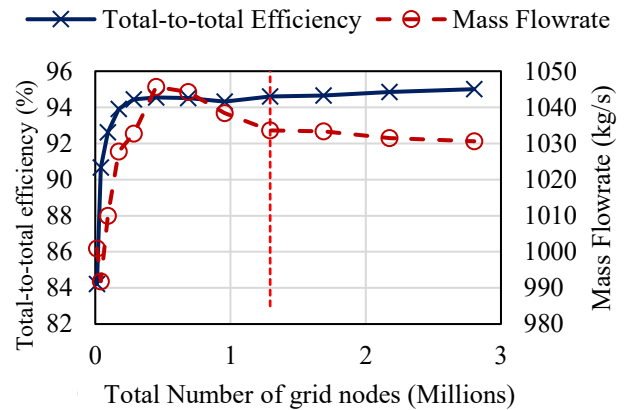
a)
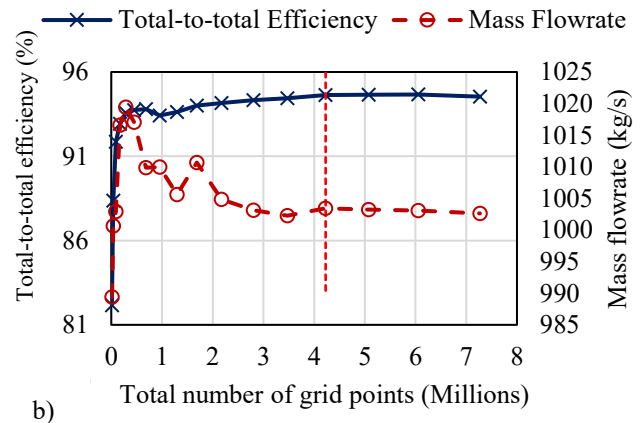
b)

FIGURE 5 MESH INDEPENDENCE STUDY, (A) k-ω SST MODEL, (B) k-ε EARSM MODEL.

Mesh independence studies have been conducted for the 9 proposed turbulence models. The results presented by Figure 6 show a comparison between the number of grid points selected as the mesh independent solution for each turbulence model. It can be seen that the fastest converging model is the SST model which is recommended by many authors [23, 30-33] in conducting numerical simulations of turbomachinery. Most of the k-ε and k-ω models show a relatively lower number of grid points compared to RSM models.
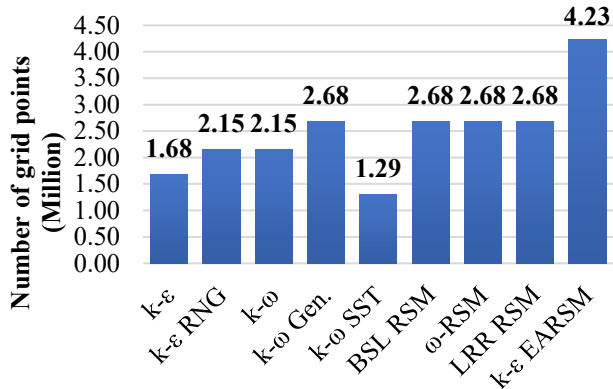
FIGURE 6 COMPARISON BETWEEN TOTAL NUMBER OF GRID POINTS IN MILLIONS FOR MESH INDEPENDENT SOLUTION

4.3 Flow Structures

To evaluate the different types of aerodynamic losses within the proposed turbine stage, the k-ω turbulence model has been selected to review the results. The k-ω model is one the most common two-equation eddy viscous RANS models which is recommended by many authors in the literature. It has been also noted that this model gives a moderate turbulence intensity and requires moderate number of grid points to give a mesh independent solution [24, 36]. The flow structure is firstly investigated by generating the blade-to-blade view presented by Figure 7 which report the Mach number distribution at the mid-span of the blades. The sudden change in the velocity magnitude at the trailing edge indicates the potential for energy loss due to the trailing edge effect in both rotor and stator blades. At the interface, upstream data are transferred to downstream the interface with the mixing plane definition where the difference between the upstream and downstream Mach number or velocity magnitudes accounts for the domain rotational speed.
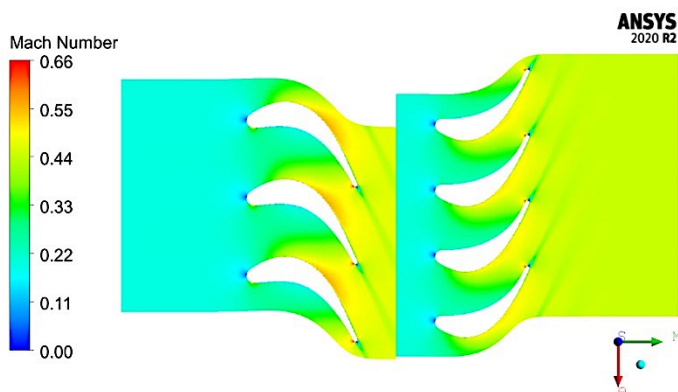

FIGURE 7 MACH NUMBER DISTRIBUTION, k-ω MODEL.

In order to investigate the turbulence downstream of the stator blades, the stator local loss coefficient is introduction to show the losses in enthalpy locally along the circumferential

location downstream the stator blades. A similar approach can be applied to the rotor to illustrate the local behaviour of the flow by introducing losses in enthalpy circumferentially. The location for the stator local loss coefficient is defined by Figure 8 (a) as a plane normal to the axial direction just downstream the stator blades which is cut with a line at 50% span. The static entropy distribution is shown in Figure 8(a) to illustrate how losses can vary locally downstream the blades as a result of the flow structure within the passage. Near the hub and shroud surfaces, the boundary layer development causes additional friction and swirl represented by the red areas near these walls which makes the entropy value increase at these regions.

It can be observed from Equation 2 that the stator loss coefficient relates the difference between the actual and isentropic enthalpies at the local point downstream the stator blades to the total difference between the stagnation enthalpy at the stator inlet and the isentropic enthalpy at the stator outlet. Figure 8 (b) shows the distribution of the stator local loss coefficient against the angle of one blade passage, which is approximately 1.6° for the total number of stator blades which is defined as 227. By integrating the local loss coefficient along the circumferential location, the total stator loss coefficient can be obtained which is found to equal 0.039.
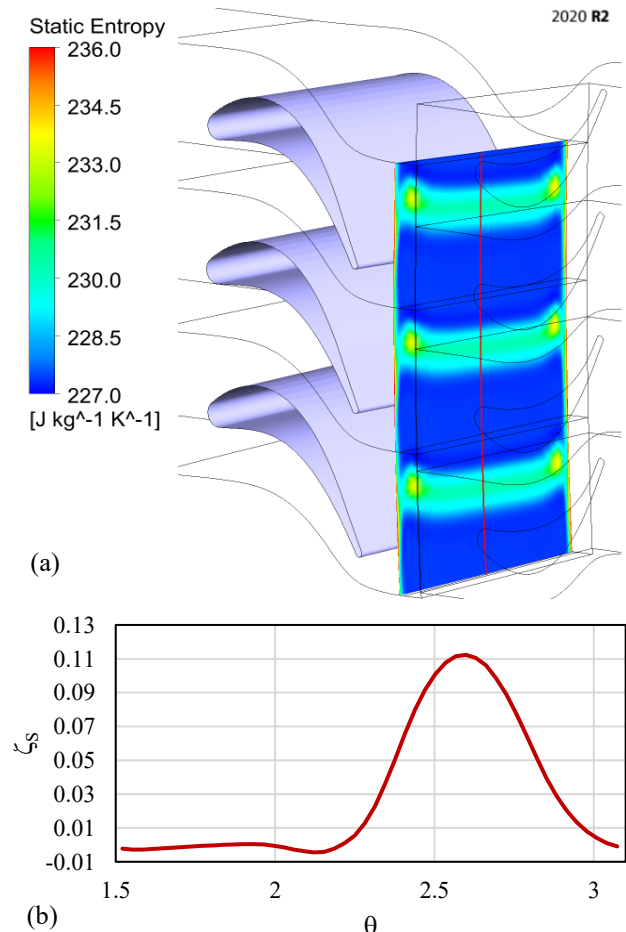

(a)

(b)

FIGURE 8 STATOR LOCAL LOSS COEFFICIENT, (A) LOCATION, (B) DISTRIBUTION OVER ONE FLOW PASSAGE AT MID-SPAN.

4.4 Loss evaluation

Losses in the turbine stage can be represented by the entropy change from inlet to outlet along the turbine axial direction. The expansion process is reported in Figure 9 on an enthalpy-entropy diagram where the aerodynamic losses can be quantified within the stator/rotor blade, stator/rotor trailing edge, the axial gap between the rotor and stator, and the exit domain downstream of the rotor blade. In order to accurately divide the total entropy generated within the proposed stage to the different domains between stator, rotor, Figure 10 is presented to show a direct relation between entropy and axial location from inlet to outlet.

A link between the two figures can be established based on the fact that the enthalpy drops occur across the stator and the rotor bladed regions and not in the rotor-stator interspace or the inlet/outlet domains. Within the interspace and outlet domain, the flow undergoes a constant pressure process where entropy increase and enthalpy increase. The associated domains are shown by red circles reported in Figure 9. Defining different domains on the h-s figure helps in determining the sources that have higher contribution to the total loss represented by ΔS. In this case, it can be noted that a significant portion of the total loss occurs within the stator-rotor interspace, as well as through the exit domain, which means that high turbulence is captured within these regions where modifications to the design or operating conditions should be made to reduce these losses.

It can be seen from Figs. 9 and 10 that the entropy generated within the whole stage is around 2.2 J/kg.K where almost 0.8 J/kg.K occurs within the stator and rotor passages. This compares to approximately 0.1 J/kg.K and 0.2 J/kg.K that is related to stator and rotor trailing edges, respectively. A large loss of 0.5 J/kg.K is then associated with both the interspace and the exit domain, which in total is nearly half the total increase across the whole stage.
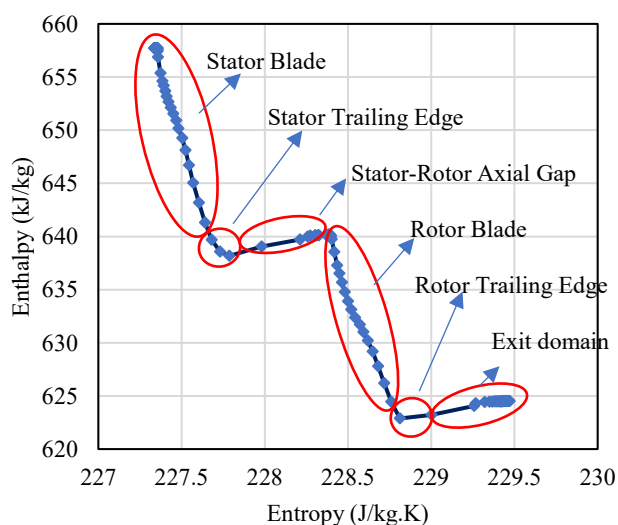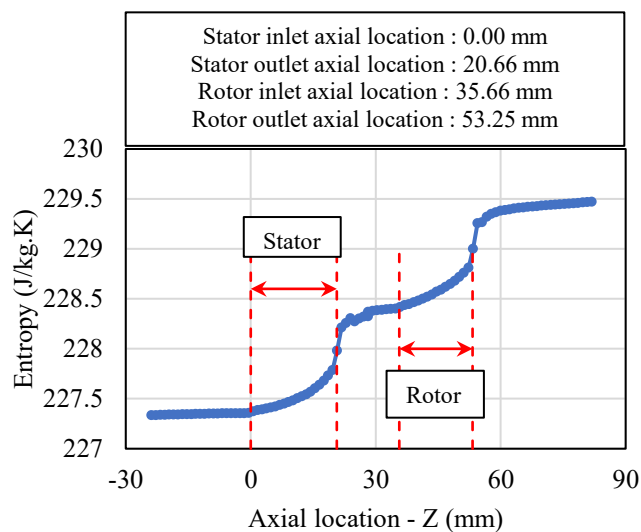
FIGURE 10 THE RELATION BETWEEN AXIAL LOCATION AND ENTROPY FROM INLET TO OUTLET

4.5 Comparison of Turbulence models

The differences between the turbulence models have been assessed based on different parameters including the mass flowrate, power, efficiencies, loss coefficients and blade loading. Various distribution figures for entropy, enthalpy and local loss coefficients have also been investigated in the following sections to show the differences in performance between the turbulence models under investigation. The comparison between absolute and relative velocities is reported by Figure 11 by introducing inlet and outlet velocity diagrams for different turbulence models. To reduce the number of curves and make the figure more clear, identical models have been eliminated. The standard k-ε, k-ε RNG, k-ω generalized and k-ε EARSM showed identical velocity diagrams and they are all represented by the EARSM model. The k-ω, k-ω SST, ω-RSM and BSL RSM models also showed identical velocity triangles and they are all represented by the k-ω model. LRR RSM models and the MLD model are included for the comparison. The results showed neglected differences between all the CFD turbulence models except for the LRR RSM model which showed a significant increase in the absolute inlet velocity to the rotor which indicates a higher expansion within the nozzle vanes. Compared to the MLD, most of the CFD models showed reasonable deviations in the absolute and relative velocities.

The expansion process represented by the fluid state at inlet, interface and outlet surfaces is represented by the h-s diagram shown in Figure 12. The figure compares the different turbulence models to the mean-line model however, some of the models under investigation are omitted to make the figure clearer. It is noted that the expansion process obtained by k-ω, k-ω generalized, k-ω SST and k-ε RNG models are nearly identical so they are all replaced with the k-ω model to represent their behaviour. The BSL RSM and ω-RSM models are also found to be identical and replaced with the BSL RSM model.

FIGURE 9 THE RELATION BETWEEN ENTHALPY AND ENTROPY FROM INLET TO OUTLET

All the remaining models, as well as the mean-line results are compared within the figure. The comparison reveals that the least amount of entropy generation among CFD models is recorded by the LRR RSM which indicates that this model predicts the least amount of turbulence within the domain. The largest entropy generation is captured by the standard k-ε model and identically the other three models mentioned earlier.
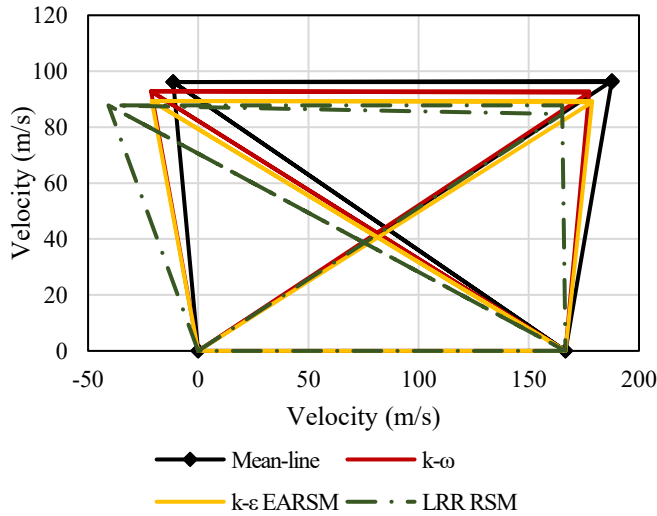

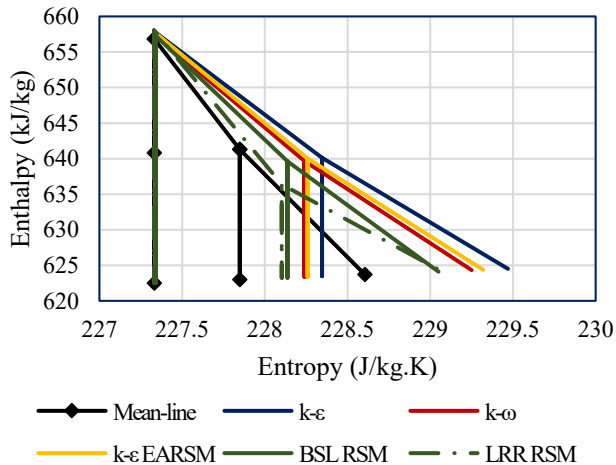*FIGURE 11 VELOCITY TRIANGLES FOR DIFFERENT TURBULENCE MODELS*

FIGURE 12 SIMPLIFIED h-s DIAGRAM FOR DIFFERENT TURBULENCE MODELS

The total-to-total efficiency and the loss coefficients are considered very important parameters in comparing the behaviour of different turbulence models. The turbine total-to-total efficiency is reported in Figure 13 while the stator and rotor loss coefficients are reported in Figure 14. The variation in total-to-total efficiency between the different turbulence models is found to be within 1.16% of the average value which

is nearly 95% compared to 96.5% in the mean-line model, while the variation in the nozzle and rotor loss coefficients are nearly 41.28% and 22.87% respectively.
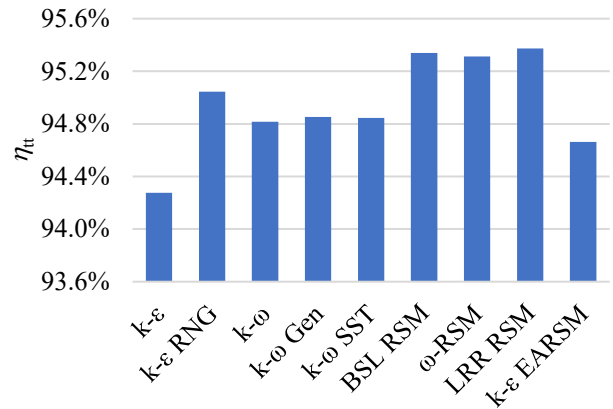

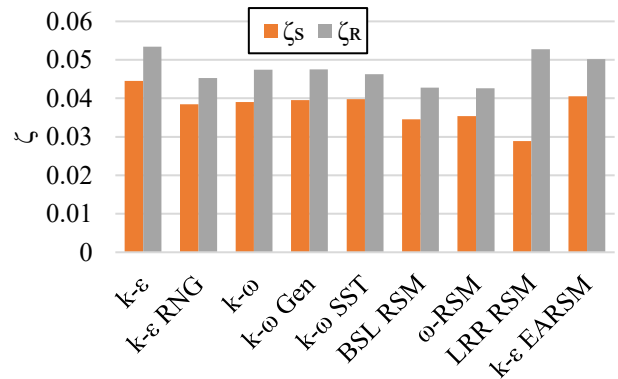*FIGURE 13 COMPARISON OF TOTAL-TO-TOTAL EFFICIENCY, FOR THE DIFFERENT TURBULENCE MODELS*

FIGURE 14 COMPARISON OF NOZZLE, AND ROTOR LOSS COEFFICIENTS FOR THE DIFFERENT TURBULENCE MODELS

Most of the RSM models predict a relatively high turbine efficiency except the k-ε based EARSM model, which means that these models have captured the least amount of secondary flows and vortices. The lowest efficiency is recorded by the standard k-ε model followed by the k-ε EARSM and the three k-ω models where more vortices are predicted. For the same reason, the highest nozzle and rotor loss coefficients are predicted by the k-ε model. The k-ε turbulence model has shown a superior performance in capturing what is called by "corner vortex" in axial compressors [37] which agrees with the presented results that this model can capture the largest number of vortices represented by the highest loss coefficients although this could be over estimating the actual flow features. The performance of k-e turbulence model is further investigate for radial turbines and showed an over-prediction of the total kinetic energy at some locations within the solution domain [38]. Simoes *et al.* [39] have shown that compared to k-ω and

k-ε models, k-ω SST results are the closest to the experimental data simulating axial flow compressor so, this model could be selected as the most suitable for accurate results.

To better understand the large deviations in loss coefficients between turbulence models, Figure 15 is presented to visualise the deviation in vortex structure between two different loss models; k-ω SST and BSL RSM by introducing the absolute helical velocity distribution which shows a slight difference between the two models within the stator blades domain while the difference grows in the rotor domain. It is expected to have a similar performance between the different turbulence models in the nozzle domain because the flow is admitted to the stage with medium turbulence intensity uniformly distributed across the inlet boundary so that no strong turbulence streams are generated within the stator domain to make the differences obvious. The rotor domain is expected to have much more turbulence as a result of the domain rotation and the turbulence generated downstream the stator blades so that the differences between the turbulence models' behaviour become more significant. The higher turbulence intensity between rotor blades agrees with the values of loss coefficients reported by Figure 14. For the same two models, the stator local loss coefficient is compared in Figure 16 where the difference in location and intensity of the wake regions are shown for each model downstream the stator blades.
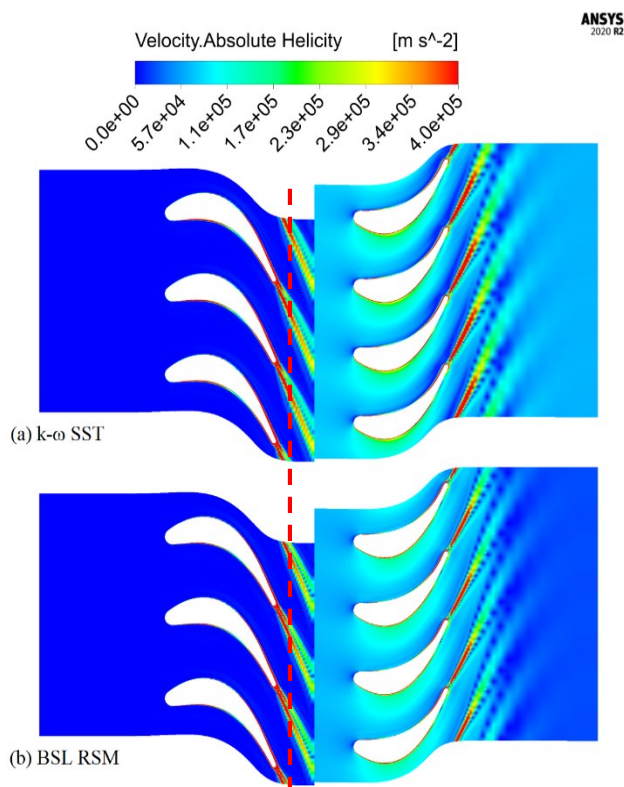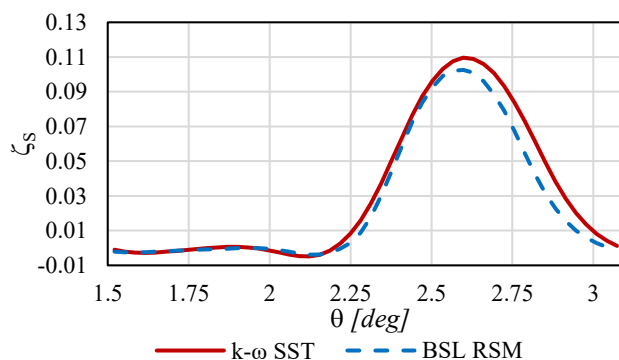

FIGURE 16 STATOR LOCAL LOSS COEFFICIENT VS. CIRCUMFERENTIAL LOCATION

A comparison between the power, mass flow rate, efficiency, loss coefficients, and blade loading is presented by Table 4. The results show that the highest power is calculated with the BSL RSM turbulence model where the same model shows the highest total to total efficiency and the lowest rotor/nozzle loss coefficients. The mass flow rate reflects the flow resistance along the flow path from inlet to outlet where the minimum obtained value is 968.23 kg/s from the LRR RSM model, and the highest value is 1059.23 kg/s obtained from the BSL RSM model.

It can be noted that the power and mass flow rate are in a good agreement as the they are directly proportional. In terms of efficiency, both total-to-total and total-to-static efficiencies have showed a slight deviation between the different turbulence models which explains the obtained very small loss coefficients in both stator and rotor. The blade loading showed a slight variation because the boundary conditions are defined with constant inlet and outlet pressures so, only slight variation in pressure along the blade appears due to the different flow structure in each turbulence model.

FIGURE 15 COMPARISON OF ABSOLUTE HELICAL VELOCITY FOR (A) k-ω SST AND, (B) BSL RSM TURBULENCE MODELS

TABLE 4 COMPARISON BETWEEN TURBULENCE MODELS

Model	Power (MW)	$\dot{m}$ (kg/s)	η_{tt}	ξ_N	ξ_R	Z
$k - \varepsilon$ Standard	33.73	1007.2	0.943	0.045	0.053	1.196
$k - \varepsilon$ RNG	34.33	1020.6	0.950	0.038	0.045	1.202
$k - \omega$	35.2	1056.8	0.948	0.039	0.047	1.19
$k - \omega$ Gen.	34.33	1022.6	0.949	0.040	0.048	1.20
$k - \omega$ SST	35.15	1054.7	0.948	0.040	0.046	1.191
BSL RSM	35.42	1059.2	0.953	0.035	0.043	1.195
ω RSM	35.31	1055.9	0.953	0.035	0.043	1.195
LRR RSM	33.14	968.2	0.954	0.029	0.053	1.223
$k - \varepsilon$ EARSM	34.14	1017.6	0.947	0.041	0.050	1.199

The amount of entropy generated is plotted against axial location and compared for all the proposed turbulence models in Figure 17. The distribution shows a horizontal line at the beginning before z=0 where the flow is nearly uniform with minimum losses within the inlet domain. A smooth increase in the entropy value is then noticed from 0 mm to 20.66 mm where the fixed blade exists which indicates minor turbulence in this area. At 20.66 mm, which is the trailing edge of the nozzle blade, a sharp increase in entropy is recorded followed by a slight increase in entropy in the axial gap between the nozzle and the rotor blade until z = 35.66 mm. The entropy again increases within the rotor blade until z = 53.25 mm, until there is a sharp increase at the rotor trailing edge. The rate of entropy generation in the rotor blade is slightly higher that the in the nozzle blade due to the increased amount of turbulence and vortices due to domain rotation and the turbulence induced by the upstream stator blade . After the rotor trailing edge, a slight increase is recorded within the exit domain due to the turbulence and swirl motion generated within the stage.

By comparing the different turbulence models, the highest final entropy value is calculated by the k-ε model followed by k-ε EARSM, k-ε RNG and k-ω models. The RSM models have presented the least entropy increase along the flow passage. In comparison between k-ε, k-ω SST and SSG RSM turbulence models in simulating the performance of radial inflow turbine presented by Singh *et al.* [38], the RSM turbulence model has shown the least satisfactory results as it presented the lowest accuracy in predicting the total kinetic energy of fluctuating motions at the impeller disc elevation. This performance is similar to the performance of the three RSM models presented in this study which showed the lowest entropy generation among the tested turbulence models.
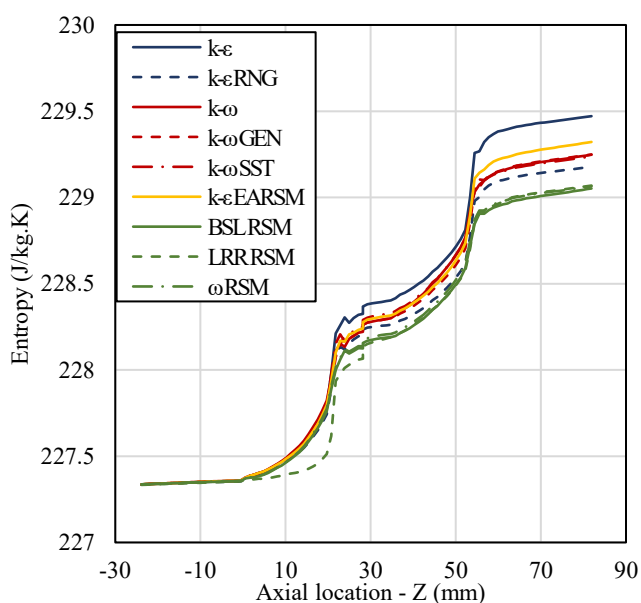
The expansion process is represented by h-s diagram shown by Figure 18 to relate the loss in power represented by entropy to the developed power represented by enthalpy. The first part of the curves indicates the expansion through the nozzle blades which is slightly sharp compared to the expansion within the rotor blades due to the lower entropy generated within the nozzle blades. The semi-horizontal lines after each blade row follows constant pressure lines on h-s charts where enthalpy increase as entropy and temperature increase. The figure shows a similar enthalpy drop for all turbulence models, which indicates a low variation in power although the entropy generated varies more significantly. This is because of the high total-to-total efficiency, which indicates that large variations in losses cause small variations in overall performance.
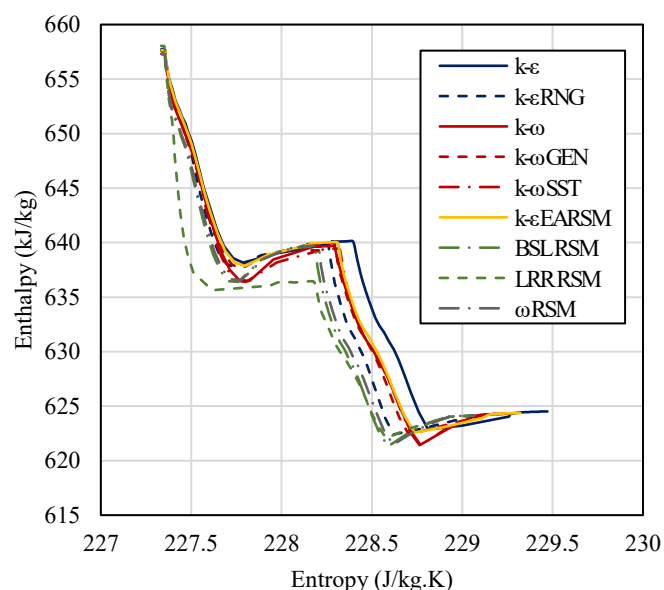

FIGURE 18 COMPARISON OF ACTUAL EXPANSION PROCESS ON h-s DIAGRAM FOR DIFFERENT TURBULENCE MODELS

4.6   Sensitivity at off-design conditions

To investigate the response of different turbulence models at off-design conditions, the rotor outlet pressure is varied while all other boundary conditions and geometric parameter are kept constant. For simplicity, 6 turbulence models are included in which are k-ε, k-ε RNG, k-ω Generalized, k-ω SST, BSL RSM and LRR RSM. It is not expected to get additional value from the excluded 3 models as the performance of the k-ω and k-ε EARSM models is found to be very close to the k-ω SST model and the performance of ω-RSM model is similar to the BSL RSM model. The relation between the stage pressure ratio and the mass-flow rate is reported by Figure 19 where it can be seen that the mass-flow rate increases as the pressure ratio increase.

The relation between the mass-flow rate and total to total efficiency for the considered turbulence models are presented

FIGURE 17 COMPARISON OF THE ENTROPY FROM INLET TO OUTLET FOR DIFFERENT TURBULENCE MODELS

in Figure 20. The results show that the k-ε RNG model is more sensitive to flow variation since the efficiency drops drastically at lower mass-flow rates compared to the other models. On the other hand, the LRR RSM model is found to be less sensitive to the mass-flow rate variation and gave the highest efficiency values at low mass-flow rates. The effect of varying mass flowrate on the rotor loss coefficient is presented by Figure 21. The results have reported a reduction in the rotor loss coefficient at high mass flowrates because the velocity levels increase within the solution domain while it can be noted the inverse proportion between the outlet rotor velocity and the rotor loss coefficient from Equation 3. No overlap between the curves has been recorded within the tested range which means that the performance of the proposed turbulence models is stable over the specified range for this study.
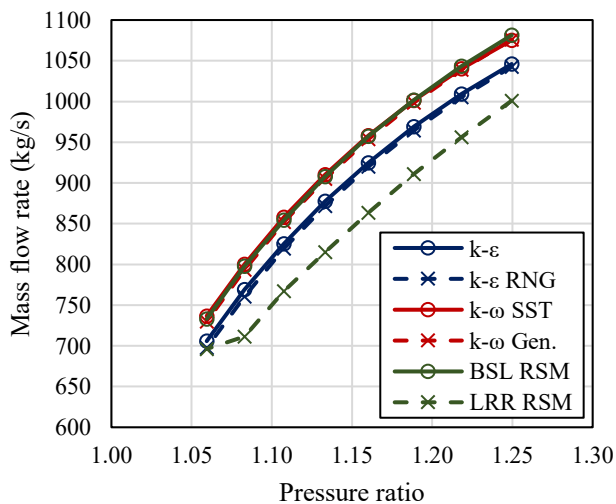

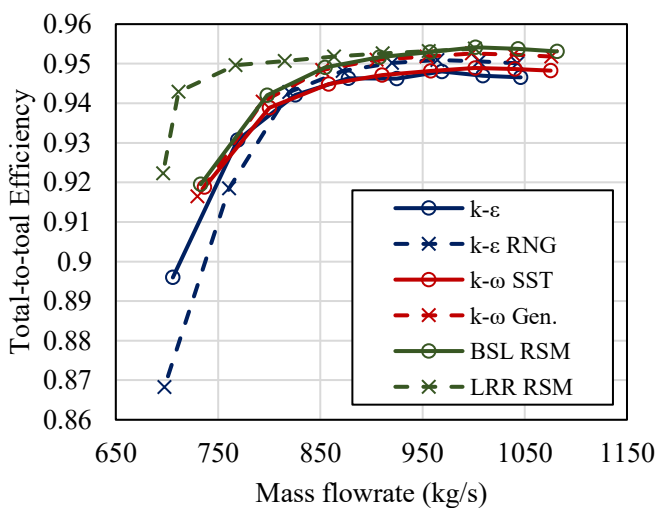*FIGURE 19 RELATION BETWEEN PRESSURE RATIO AND MASS FLOWRATE FOR DIFFERENCE TURBULENCE MODELS*

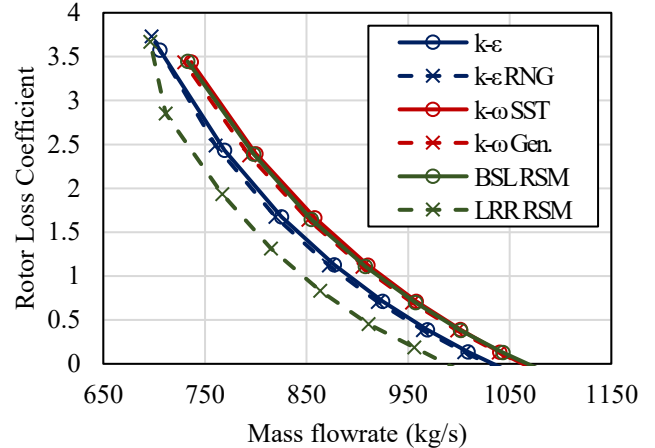*FIGURE 20 THE EFFECT OF VARYING MASS FLOWRATE ON TOTAL-TO-TOTAL EFFICIENCY*

FIGURE 21 THE EFFECT OF VARYING MASS FLOWRATE ON ROTOR LOSS COEFFICIENT

To understand the differences in performance at off-design operating condition, the flow structure is compared for the LRR RSM, k-ω SST and k-ε RNG turbulence models at a pressure ratio of 1.08. Figure 22 shows the static entropy distribution at a location just downstream the stator and rotor blades at 50% span for the three mentioned turbulence models. The comparison provides a description to the aerodynamic loss represented by entropy generation which is found to be the highest in the RNG model for both stator and rotor blades and the lowest for the LRR RSM model. These results are in good agreement with the efficiency values mentioned in Figure 20 where the highest total to total efficiency is recorded with the LRR turbulence model at this operating point which reflects the least losses captured. The change in peak location can give an approximate indication of differences in flow angles between the three models which is less than 0.3 and 0.1 degrees at the stator and rotor outlets, respectively.
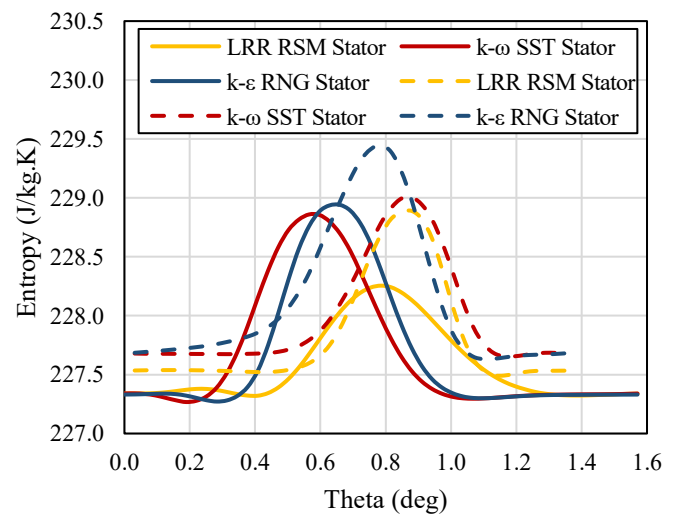

FIGURE 22 COMPARING THE ENTROPY DISTRIBUTION LOCALLY DOWNSTREAM OF THE STATOR AND ROTOR BLADES AT 50% SPAN.

5 CONCLUSION

This paper has investigated the sensitivity of CFD performance predictions for turbomachinery operating with CO_2-based mixtures to the turbulence model selected. Nine different turbulence models have been implemented to simulate an axial turbine stage operating with a CO_2-$TiCl_4$ mixture, which is a promising working fluid for transcritical CO_2 power cycles intended for CSP plants. To compare the turbulence models, turbine stage performance is evaluated through an assessment of both loss coefficients and efficiencies alongside a comparison of the flow structures predicted by each turbulence model at design and off-design operating conditions.

The CFD simulations are verified against a mean-line model based on Soderberg's correlations, which provide estimates for rotor and stator loss coefficients. Both models are in a good agreement for mass-flow rate, power, velocities, blade loading and efficiencies, although the loss coefficients differ due to the inherent differences between the two approaches.

According to the results, it is concluded that:

- Based on the mesh independence studies, the model which required the least computational power to achieve a mesh independent solution is k-ω SST followed by the standard k-ε model. The k-ε EARSM model required the largest grid size to obtain a grid-independent solution.
- The comparison between the different turbulence models has shown that the largest stator and rotor loss coefficients are predicted by the k-ε model followed by the k-ε EARSM and the three k-ω models. On the other hand, the BSL RSM, w RSM and LRR RSM models predict the least turbulence within the flow field, the highest total to total efficiency and the lowest loss coefficients.
- The results of loss estimation represented by entropy increase along the axial location have shown a significant increase of entropy in the stator-rotor interspace and exit domain compared to the entropy generated within the rotor and stator passaged. These losses should be minimized.
- Due to the high total to total efficiency, negligible variation in power output has been observed between the different turbulence models, even though the stator and rotor loss coefficients vary considerably.

At off-design operating conditions, the pressure at the rotor outlet has been varied and the change in mass-flow rate, stage efficiency and the loss coefficients has been determined. The sensitivity analysis reveals that the k-ε RNG model is the most sensitive at low flow rates while the LRR RSM model has shown the least sensitivity to the mass flow rate change. The overall response of the different turbulence models shows a sharp drop in total-to-total efficiency when the pressure ratio, and hence mass-flow rate, is reduced. The efficiency drop recorded using the k-ε RNG model is 8.24% at a mass flowrate reaching 30% off-design compared to 3.1% drop in efficiency for the LRR RSM model.

6 REFERENCES

[1] Binotti, Marco, Di Marcoberardino, Gioele, Iora, Paolo, Invernizzi, Costante Mario and Manzolini, Giampaolo. "Supercritical carbon dioxide/alternative fluids blends for efficiency upgrade of solar power plant." *3rd European Conference on Supercritical CO2 (sCO2) Power Systems 2019: 19th-20th September 2019*. pp. 222-229.

[2] Al-Sulaiman, Fahad A. and Atif, Maimoon. "Performance comparison of different supercritical carbon dioxide Brayton cycles integrated with a solar power tower." *Energy* Vol. 82 (2015): pp. 61-71.

[3] Manzolini, Giampaolo, Binotti, Marco, Bonalumi, Davide, Invernizzi, Costante and Iora, Paolo. "CO2 mixtures as innovative working fluid in power cycles applied to solar plants. Techno-economic assessment." *Solar Energy* Vol. 181 (2019): pp. 530-544. https://doi.org/10.1016/j.solener.2019.01.015.

[4] Bonalumi, D., Lasala, S. and Macchi, E. "CO2-TiCl4 working fluid for high-temperature heat source power cycles and solar application." *Renewable Energy* Vol. 147 (2020): pp. 2842-2854. https://doi.org/10.1016/j.renene.2018.10.018.

[5] Lasala, S., Bonalumi, D., Macchi, E., Privat, R. and Jaubert, J. N. "The design of CO2-based working fluids for high-temperature heat source power cycles." *Energy Procedia* Vol. 129 (2017): pp. 947-954. https://doi.org/10.1016/j.egypro.2017.09.125.

[6] Salah, Salma I, Khader, Mahmoud A, White, Martin T and Sayma, Abdulnaser I. "Mean-Line Design of a Supercritical CO2 Micro Axial Turbine." *Applied Sciences* Vol. 10 No. 15 (2020): pp. 5069.

[7] Jang, Hyuck Jun, Kang, Soo Young, Lee, Jeong Jin, Kim, Tong Seop and Park, Seong Jin. "Performance analysis of a multi-stage ultra-supercritical steam turbine using computational fluid dynamics." *Applied Thermal Engineering* Vol. 87 (2015): pp. 352-361. 10.1016/j.applthermaleng.2015.05.007.

[8] Langston, Lee. "Secondary Flows in Axial Turbines—A Review." *Annals of the New York Academy of Sciences* Vol. 934 (2001): pp. 11-26. 10.1111/j.1749-6632.2001.tb05839.x.

[9] Denton, Jd and Xu, L. "The trailing edge loss of transonic turbine blades." (1990).

[10] Trindade, Daniel Back, Bugała, Pamela and Simone, Domenico. "Review of loss models for high pressure turbines." *Journal of KONES* Vol. 25 No. 2 (2018): pp. 37-44.

[11] Dunham, J and Came, Pm. "Improvements to the Ainley-Mathieson method of turbine performance prediction." (1970).

[12] Kacker, Sc and Okapuu, U. "A mean line prediction method for axial flow turbine efficiency." (1982).

[13] Craig, Hrm and Cox, Hja. "Performance estimation of axial flow turbines." *Proceedings of the Institution of Mechanical Engineers* Vol. 185 No. 1 (1970): pp. 407-424.

[14] Moustapha, Sh, Kacker, Sc and Tremblay, B. "An improved incidence losses prediction method for turbine airfoils." (1990).

[15] Ennil, Ali Bahr, Al-Dadah, Raya, Mahmoud, Saad, Rahbar, Kiyarash and Aljubori, Ayad. "Minimization of loss in small scale axial air turbine using CFD modeling and

evolutionary algorithm optimization." *Applied Thermal Engineering* Vol. 102 (2016): pp. 841-848. 10.1016/j.applthermaleng.2016.03.077.

[16] Ennil, A. S. Bahr, Al-Dadah, R. K., Mahmoud, S., Al-Jubori, A. M. and Rahbar, K. "Prediction of Losses in Small Scale Axial Air Turbine Based on CFD Modelling." *Energy Procedia* Vol. 75 (2015): pp. 3271-3276. https://doi.org/10.1016/j.egypro.2015.07.702.

[17] Ainley, Dg and Mathieson, G Cr, 1951, "A method of performance estimation for axial-flow turbines," AERONAUTICAL RESEARCH COUNCIL LONDON (UNITED KINGDOM).

[18] Schmitt, François G. "About Boussinesq's turbulent viscosity hypothesis: historical remarks and a direct evaluation of its validity." *Comptes Rendus Mécanique* Vol. 335 No. 9-10 (2007): pp. 617-627.

[19] Bakker, André, 2008, "Lectures on Applied Computational Fluid Dynamics," www.bakker.org. Bakker, André, 2008, "Lectures on Applied Computational Fluid Dynamics."

[20] Noori Rahim Abadi, S. M. A., Ahmadpour, A., Abadi, S. M. N. R. and Meyer, J. P. "CFD-based shape optimization of steam turbine blade cascade in transonic two phase flows." *Applied Thermal Engineering* Vol. 112 (2017): pp. 1575-1589. 10.1016/j.applthermaleng.2016.10.058.

[21] Francesco, Giacomelli, Federico, Mazzelli and Adriano, Milazzo. "CFD modelling of the condensation inside a cascade of steam turbine blades: comparison with an experimental test case." *Energy Procedia* Vol. 126 No. 5 (2017): pp. 730-737. 10.1016/j.egypro.2017.08.306.

[22] Hu, Pengfei, Cao, Lihua, Su, Jingkai, Li, Qi and Li, Yong. "Distribution characteristics of salt-out particles in steam turbine stage." *Energy* Vol. 192 (2020): pp. 116626. 10.1016/j.energy.2019.116626.

[23] Morgese, Gaetano, Torresi, Marco, Fortunato, Bernardo and Camporeale, Sergio Mario. "Optimized Aerodynamic Design of Axial Turbines for Waste Energy Recovery." *Energy Procedia* Vol. 82 (2015): pp. 194-200. 10.1016/j.egypro.2015.12.019.

[24] Touil, Kaddour and Ghenaiet, Adel. "Simulation and analysis of vane-blade interaction in a two-stage high-pressure axial turbine." *Energy* Vol. 172 (2019): pp. 1291-1311. 10.1016/j.energy.2019.01.111.

[25] Han, Wanlong, Zhang, Yifan, Li, Hongzhi, Yao, Mingyu, Wang, Yueming, Feng, Zhenping, Zhou, Dong and Dan, Guangju. "Aerodynamic design of the high pressure and low pressure axial turbines for the improved coal-fired recompression SCO2 reheated Brayton cycle." *Energy* Vol. 179 (2019): pp. 442-453.

[26] Shi, Dongbo, Zhang, Lei, Xie, Yonghui and Zhang, Di. "Aerodynamic design and off-design performance analysis of a multi-stage S-CO2 axial turbine based on solar power generation system." *Applied Sciences* Vol. 9 No. 4 (2019): pp. 714.

[27] Zhou, Kehan, Wang, Jiangfeng, Xia, Jiaxi, Guo, Yumin, Zhao, Pan and Dai, Yiping. "Design and performance analysis of a supercritical CO2 radial inflow turbine." *Applied Thermal Engineering* Vol. 167 (2020): pp. 114757. https://doi.org/10.1016/j.applthermaleng.2019.114757.

[28] Holaind, Norman, Bianchi, Giuseppe, De Miol, Maxence, Saravi, Samira Sayad, Tassou, Savvas A., Leroux, Arthur and Jouhara, Hussam. "Design of radial turbomachinery for supercritical CO 2 systems using theoretical and numerical CFD methodologies." *Energy Procedia* Vol. 123 (2017): pp. 313-320. 10.1016/j.egypro.2017.07.256.

[29] Ameli, Alireza, Uusitalo, Antti, Turunen-Saaresti, Teemu and Backman, Jari. "Numerical Sensitivity Analysis for Supercritical CO 2 Radial Turbine Performance and Flow Field." *Energy Procedia* Vol. 129 (2017): pp. 1117-1124. 10.1016/j.egypro.2017.09.233.

[30] Vatanmakan, Masoud, Lakzian, Esmail and Mahpeykar, Mohammad Reza. "Investigating the entropy generation in condensing steam flow in turbine blades with volumetric heating." *Energy* Vol. 147 (2018): pp. 701-714. 10.1016/j.energy.2018.01.097.

[31] Lv, Guochuan, Yang, Jinguang, Shao, Wenyang and Wang, Xiaofang. "Aerodynamic design optimization of radial-inflow turbine in supercritical CO2 cycles using a one-dimensional model." *Energy Conversion and Management* Vol. 165 (2018): pp. 827-839. https://doi.org/10.1016/j.enconman.2018.03.005.

[32] Keep, Joshua A., Vitale, Salvatore, Pini, Matteo and Burigana, Matteo. "Preliminary verification of the open-source CFD solver SU2 for radial-inflow turbine applications." *Energy Procedia* Vol. 129 (2017): pp. 1071-1077. 10.1016/j.egypro.2017.09.130.

[33] Obert, Benoit and Cinnella, Paola. "Comparison of steady and unsteady RANS CFD simulation of a supersonic ORC turbine." *Energy Procedia* Vol. 129 (2017): pp. 1063-1070. 10.1016/j.egypro.2017.09.122.

[34] Neises, T and Turchi, C. "A comparison of supercritical carbon dioxide power cycle configurations with an emphasis on CSP applications." *Energy Procedia* Vol. 49 (2014): pp. 1187-1196.

[35] Binotti, Marco, Astolfi, Marco, Campanari, Stefano, Manzolini, Giampaolo and Silva, Paolo. "Preliminary assessment of sCO2 cycles for power generation in CSP solar tower plants." *Applied Energy* Vol. 204 (2017): pp. 1007-1017.

[36] Zhou, Chao, Hodson, Howard and Himmel, Christoph. "The Effects of Trailing Edge Thickness on the Losses of Ultrahigh Lift Low Pressure Turbine Blades." *Journal of Turbomachinery* Vol. 136 No. 8 (2014). 10.1115/1.4026456.

[37] Liu, Yangwei, Yu, Xianjun and Liu, Baojie. "Turbulence models assessment for large-scale tip vortices in an axial compressor rotor." *Journal of Propulsion and Power* Vol. 24 No. 1 (2008): pp. 15-25.

[38] Singh, Harminder, Fletcher, David F and Nijdam, Justin J. "An assessment of different turbulence models for predicting flow in a baffled tank stirred with a Rushton turbine." *Chemical Engineering Science* Vol. 66 No. 23 (2011): pp. 5976-5988.

[39] Simoes, Marcelo R, Montojos, Bruno G, Moura, Newton R and Su, Jian. "Validation of turbulence models for simulation of axial flow compressor." *20th International Congress of Mechanical Engineering*.